Published in final edited form as:
Ann Thorac Surg. 2010 January ; 89(1): 132–137. doi:10.1016/j.athoracsur.2009.08.075.

Effect of adjustable passive constraint on the failing left ventricle: A finite element model study

Choon-Sik Jhun, PhD[1,3], **Jonathan F. Wenk, PhD**[1,3], **Zhihong Zhang, MS**[1,3], **Samuel T. Wall PhD**[1,3], **Kay Sun, PhD**[1,3], **Hani N. Sabbah, PhD**[4], **Mark B. Ratcliffe, MD**[1,2,3], and **Julius M. Guccione, PhD**[1,2,3]

[1]Department of Surgery, University of California, San Francisco, California

[2]Department of Bioengineering, University of California, San Francisco, California

[3]Department of Veterans Affairs Medical Center, San Francisco, California

[4]Henry Ford Hospital, Detroit, MI

Abstract

Background—Passive constraint is used to prevent left ventricular (LV) dilation and subsequent remodeling. However, there has been concern about the effect of passive constraint on diastolic LV chamber stiffness and pump function. This study determined the relationship between constraint, diastolic wall stress, chamber stiffness and pump function. We tested the hypothesis that passive constraint at 3 mmHg reduces wall stress with minimal change in pump function.

Methods—"A 3-dimensional finite element model of the globally dilated LV based on LV dimensions obtained in dogs that had undergone serial intracoronary microsphere injection was created. The model was adjusted to match experimentally observed end-diastolic LV volume and mid-ventricular wall thickness. The experimental results used to create the model were previously reported.

A pressure of 3, 5, 7, and 9 mmHg was applied to the epicardium. Fiber stress, end-diastolic pressure volume relationship (EDPVR), end-systolic pressure volume relationship (ESPVR) and the stroke volume end-diastolic pressure (Starling) relationship were calculated."

Results—As epicardial constraint pressure increased, fiber stress decreased, the EDPVR shifted to the left and the Starling relationship shifted down and to the right. The ESPVR did not change. A constraining pressure of 2.3 mm Hg was associated with a 10% reduction in stroke volume and mean end-diastolic fiber stress was reduced by 18.3% (Inner wall), 15.3% (Mid wall), and 14.2% (Outer wall).

Conclusion—Both stress and cardiac output decrease in a linear fashion as the amount of passive constraint is increased. If the reduction in cardiac output is to be less than 10%, passive constraint should not exceed 2.3 mmHg. On the other hand, this amount of constraint may be sufficient to reverse eccentric hypertrophy after myocardial infarction.

Keywords

Passive constraint device; wall stress; pump function

Corresponding Author: Mark Ratcliffe, MD, Surgical Service (112), San Francisco Veterans Affairs Medical Center, 4150 Clement Street, San Francisco, California 94121, mark.ratcliffe@va.gov, Telephone: (415) 221-4810. FAX: (415) 750-2181.

Introduction

Both myocardial infarction [1] and volume loading associated with regurgitant valve lesions [2] lead to eccentric left ventricular hypertrophy. The mechanism is presumed to be positive feedback between diastolic LV wall stress and eccentric LV hypertrophy. [2] Further, in each case, an increase in LV size is an important adverse prognostic finding. [3-5]

The experience with skeletal muscle cardiomyoplasty [6] led to the hypothesis that passive constraint of LV enlargement would interrupt the diastolic stress/ eccentric hypertrophy cycle and halt and possibly reverse LV remodeling. A number of passive constraint devices have been used including the Acorn CorCap™ fabric 'jacket' [7], the Paracor [8] and the fluid filled balloon described by Ghanta and colleagues. [9] Experience has been greatest with the Acorn device which has been shown to reduce end-diastolic volume [10,11], shear strain [11], and infarct area. [12]

On the other hand, there has been concern about the effect of passive constraint on diastolic LV chamber stiffness and pump function. To quantify this effect, Ghanta and associates placed a fluid filled balloon around the LV. [9] In that study, a balloon pressure of 3 mmHg caused no acute change in mean aortic pressure but reduced tension time index and pressure volume area by 12 and 20% respectively. There was an acute 10% reduction in cardiac output [9] although this was not confirmed in a subsequent study [13]. Furthermore, Ghanta found that passive constraint with their device caused a 30% reduction in LV end-diastolic volume 8 weeks after device application in sheep that had remodeled after occlusion of left anterior descending diagonal coronary arteries 1 and 2. [9] Although LV mass was not measured per se, these results suggest a reduction in eccentric hypertrophy.

We used a realistic 3-D FE model to calculate the effect of the adjustable passive constraint on a failing canine heart. Our purpose was to confirm the findings of Ghanta et al. [9] and to determine the relationship between constraint, diastolic wall stress, diastolic chamber stiffness and pump function. We tested the hypothesis that passive constraint at 3 mmHg reduces diastolic wall stress without a change in pump function (Starling's law).

Methods

Finite Element Model

A 3-dimensional finite element model of the globally dilated LV based on LV dimensions obtained in dogs that had undergone serial intracoronary microsphere injection was created. [14,15] The model was adjusted to match experimentally observed end-diastolic LV volume [16] and mid-ventricular wall thickness. The experimental results used to create the model were previously reported.

The geometry of this model consisted of an axisymmetric prolate spheroid with a focus of 2.25 cm and a diameter-to-length ratio of 0.702 The muscle fiber direction throughout the LV was presumed to vary linearly in the transmural direction at 60° from the circumferential direction to the subendocardium, then at -60° from the circumferential direction to the epicardium. [17] The myocardial wall was refined into 16x5x1 (longitudinal x transmural x circumferential) 3-D cubic hermite elements with myofiber angles assigned at element nodes. A small 1 degree apical hole is included in the mesh to prevent computational singularities. The model of the unloaded state of a dilated LV is shown in Figure 1. An implicit FE solver for large deformations (CMISS) was used to simulate the end-diastolic and end-systolic state. The mesh refinement study revealed the mesh was sufficient in obtaining a converged solution.

Implementation of Passive Constraint

The levels of passive constraint, 3, 5, 7, and 9 mmHg, were implemented by applying inward pressure on the epicardium. Figure 2 shows the hydrostatic pressure loading profile acting on the epicardium and simulating passive constraint.

Boundary and Loading Conditions

At the epicardial surface of the base, all displacements were constrained. The inner basal nodes were free to move in the radial direction. End-systolic pressure (ESP) of 90 mmHg and end-diastolic pressure (EDP) of 17 mmHg were applied outwards at the inner endocardial wall. End-diastolic volume (EDV) and end-systolic volume (ESV) with no constraint nearly matched the experimental observations of 65 ml and 45 ml, respectively.

Passive Material Properties

The passive myocardium was described by a strain energy function, W, that is transversely isotropic with respect to the local fiber direction [18],

$$W=\frac{C}{2}\left(\exp^{b_f\,E_{11}^2+b_t\left(E_{22}^2+E_{33}^2+E_{23}^2+E_{32}^2\right)+b_{fs}\left(E_{12}^2+E_{21}^2+E_{13}^2+E_{31}^2\right)}-1\right) \tag{1}$$

where C, bf, bt and bfs are diastolic myocardial material parameters. E_{11} is strain in fiber direction, E_{22} is cross-fiber in-plane strain, E_{33} is radial strain transverse to the fiber direction, and the rest are shear strains. Material constants b_f, b_t, and b_{fs} were chosen as 18.48, 3.58, and 1.627. [18] The material constant, C, was selected to be 0.855 kPa, enabling us to obtain the prescribed EDV.

Active Materials Properties

Systolic contraction was modeled as the sum of the passive stress derived from the strain energy function and an active fiber directional component, $\mathbf{T_0}$, which is a function of time, t, peak intracellular calcium concentration, Ca_0, sacromere length, l, and maximum isometric tension achieved at the longest sacromere length, T_{max} [19],

$$\mathbf{S}=p\,J\mathbf{C}^{-1}+2J^{-2/3}\,\mathrm{Dev}\left(\frac{\partial\,\tilde{W}}{\partial\mathbf{C}}\right)+\mathbf{T_0}\,\{t,Ca_0,l,T_{\max}\} \tag{2}$$

where **S** is the second Piola-Kirchoff stress tensor, p is the hydrostatic pressure introduced as the Lagrange multiplier needed to ensure incompressibility and was calculated from the bulk modulus of water, J is the Jacobian of the deformation gradient tensor, **C** is the right Cauchy-Green deformation tensor, Dev is the deviatoric projection operator and W is the deviatoric contribution of the strain energy function, W (Equation 1).

The relationship between active tension, $\mathbf{T_0}$, and calcium concentration has been previously described. [19] The material constants for active contraction were $(Ca_0)_{\max}$ = 4.35 μmol/L, B = 4.75 μm^{-1}, l_0 = 1.58 μm, m = 1.0489 sec μm^{-1}, b = -1.429 sec, and l_R = 1.85 μm, where $(Ca_0)_{\max}$ is the maximum peak intracellular calcium concentration, B is a constant, l_0 is the sarcomere length at which no active tension develops and l_R is the stress-free sarcomere length. [18] To achieve the prescribed ESV, T_{max} = 128 kPa and Ca_0 = 4.35 μmol/l were chosen to represent the weakly contracting, failing ventricle. Based on the biaxial stretching experiments [20] and FE analyses [21,22], cross-fiber, in-plane stress equivalent to 40% of that along the myocardial fiber direction was added.

Calculation of End-Diastolic Pressure-Volume Relationship (EDPVR) and End-Systolic Pressure-Volume Relationships (ESPVR)

Diastolic and end-systolic solutions were obtained at ranges of end-diastolic (from 0 to 17 mmHg) and end-systolic (from 10 to 90 mmHg) chamber pressures. The ESP and ESV, determined from the FE model were fit to a linear equation by means of least square regression analysis [23],

$$ESP = E_{ES}\ (ESV - V_0) \tag{3}$$

where V_0 is the volume intercept and E_{ES} is the slope of the left ventricle elastance. The EDP and EDV, determined from the FE model were fit to the following quadratic equations using least square regression analysis [23],

$$EDP = \beta_0 + \beta_1 EDV + \beta_2 EDV^2 \tag{4}$$

where β_0, β_1, and β_2 are the stiffness parameters of the left ventricle diastolic compliance.

Calculation of Stroke Volume/EDP (Starling) Relationship

For each level of passive constraint, the stroke volume (SV) versus the EDP (Starling) relationship was calculated from diastolic and systolic pressure-volume regression. Arterial elastance, E_A, for each level of constraint was calculated according to the following equation [24]:

$$SV = \frac{EDV - V_0}{1 + E_A / E_{ES}} \tag{5}$$

where *SV* is the stroke volume, *EDV* is the volume intercept of the arterial elastance, V_0 is the volume intercept of end-systolic elastance, and E_{ES} is the slope of end-systolic elastance shown in equation 3.

Results

Using our FE model we could describe detailed average wall stress distribution and the LV pump function associated with different levels of passive constraint on the failing canine LV.

Ventricular Volumes vs. Passive Constraints

Ventricular volumes and ejection fraction associated with linearly increasing constraint are shown in Table 1. With no constraint, EDV and ESV resulted in 65.27 ml and 44.91 ml. The EDV was reduced sequentially and SV had a trend similar to EDV. The ESV was relatively unaffected across all constraint levels.

EDPVR, ESPVR and the Starling Relationship

The effect of passive constraint on diastolic compliance is shown in Table 2. The compliance curves shift to the left as the level of constraint increases (Figure 3). With no constraint, the end-systolic elastance, E_{ES}, was 3.762 mmHg/ml and the volume intercept, V_0, was 20.91 ml. The adjustable passive constraint on the stroke volume and end-diastolic pressure relationship (Starling relationship) causes progressive decrement of stroke volume at the same end-diastolic pressure (Figure 4).

End-Diastolic and End-Systolic Fiber Stress

The mean volume weighted end-diastolic fiber stress was reduced due to the application of passive constraint (Figure 5). If the reduction in cardiac output is to be less than 10%, passive constraint should be less than 2.3 mmHg (Figure 6). At that level of constraint, end-diastolic fiber stress was reduced by 18.3% (Inner wall), 15.3% (Mid wall), and 14.2% (Outer wall) relative to the case without constraint. At 7 and 9 mmHg of constraint the fiber stress at the inner wall was reduced by 54.7% and 67.6%, respectively. The average end-systolic fiber stress was minimally affected at any level of constraint.

Comments

The principal finding of this study is that both stress and cardiac output decrease in a linear fashion as the amount of passive constraint is increased. Although no amount of pump function reduction is desirable, a small decrease may be acceptable if it leads to reverse remodeling and improved systolic function. According to the numerical model, if the reduction in cardiac output is to be less than 10%, passive constraint should not exceed 2.3 mmHg. At that level of constraint, mean end-diastolic fiber stress was reduced by 18.3% (Inner wall), 15.3% (Mid wall), and 14.2% (Outer wall) relative to the case without constraint. Of note, these findings are remarkably similar to the findings of Ghanta and associates. [9] In that study, a constraint of 3 mmHg was associated with an approximate reduction in cardiac output of 10%. [9]

Diastolic Stress Reduction and the Reversal of Eccentric Hypertrophy

We know that eccentric hypertrophy is reduced after valve replacement for aortic and mitral regurgitation [7,25] and there is at least one anecdotal report of reverse remodeling of dilated cardiomyopathy during tamponade. [26]

However, until the study by Ghanta et al. [13] coupled with our subsequent analysis, the magnitude of diastolic stress reduction necessary to reduce LV hypertrophy was unknown. Our reasoning is as follows: Ghanta and colleagues showed that sustained application of an epicardial pressure of 3 mm Hg led to a 30% reduction in LV end-diastolic volume 8 weeks after device implantation. Although LV mass was not measured per se, these results suggest a reduction in eccentric hypertrophy. Our finite element model shows that an epicardial pressure of 2.3 mm Hg reduces LV end-diastolic fiber stress by between 14.2% (Outer wall) and 18.3% (Inner wall) to 4.897 kPa (Outer wall) and 6.814 kPa (Inner wall) respectively. Our conclusion is that, end-diastolic fiber stress reduction of this magnitude is sufficient to reduce eccentric hypertrophy.

Passive Constraint and Pump Function

We found that cardiac output decreases in a linear fashion as the amount of passive constraint is increased. Therefore, there is no amount of passive constraint that does not produce an acute decrease in cardiac output. This does not mean that cardiac output must be depressed in the long term after passive constraint is applied. If the reverse remodeling leads to an improvement in systolic function, cardiac output may be maintained or increased. Although the chronic end-systolic volume was not presented by Ghanta and colleagues, ejection fraction increased while end-diastolic volume remained stable suggesting a reduction in end-systolic volume. [13]

Modeling of Other Passive Ventricular Constraint Devices

The finite element model used in this study should be able to simulate the effect of Acorn and Paracor devices. However, it will be first necessary to test the materials used in those devices and incorporate those measurements in appropriate constitutive relationships. This

will not be trivial since both Acorn [27] and Paracor [8] materials are anisotropic and open mesh. The later fact means that continuum mechanics cannot be used directly. Continuum theory is based on the assumption that the distance between the particles that make up a material is much smaller than the overall dimension of the bulk material, i.e., the body is entirely occupied and the microstructure is ignored. [28] For the Acorn fabric and Paracor mesh, the discrete nature of the material means that an alternative approach must be taken to approximate the averaged material properties.

Model Limitations

In this study, only the LV was modeled. This is important since, in practice, the device wraps around both the LV and RV. For a number of reasons, the simple FE model employed in this study is not able to incorporate the RV or RV effect. While it is encouraging to see close agreement between our findings and the experimental study by Ghanta and colleagues [9], we do not assume that the RV effect is negligible. We plan future finite element studies that will include the RV.

Also, the observations made by the model reflect the results only at the time of implant of the device. The model is unable to take reactive changes in diastolic filling, autonomic tone or changes at the molecular and cellular level into consideration. [16]

Summary and Future Directions

In conclusion, we found that both stress and cardiac output decrease in a linear fashion as the amount of passive constraint is increased. If the reduction in cardiac output is to be less than 10%, passive constraint should not exceed 2.3 mm Hg. At that level of constraint, mean end-diastolic fiber stress was reduced by 18.3% (Inner wall), 15.3% (Mid wall), and 14.2% (Outer wall) relative to the case without constraint. Of considerable importance, that level of diastolic stress reduction appears sufficient to reverse eccentric hypertrophy after MI.

Future modeling studies should include the effect of different LV size and shape and different constitutive parameter values for defining passive and/or active myocardial material properties to mimic early, mid, and end-stage heart failure. Future modeling studies should include the right ventricle as well. In addition, our results need to be confirmed by comparison with experimental measurements of regional three-dimensional myocardial strain and muscle fiber orientation using tagged magnetic resonance images and magnetic resonance diffusion tensor imaging, respectively. The eventual goal would be a trial in patients with systolic heart failure.

Acknowledgments

This work was supported by grant 5R01 HL077921 (J.M.G), 5R01 HL063348 (Mark B. Ratcliffe), and P41 RR08605 from the National Institutes of Health.

References

1. Anand IS, Liu D, Chugh SS, et al. Isolated myocyte contractile function is normal in postinfarct remodeled rat heart with systolic dysfunction. Circulation 1997;96(11):3974–84. [PubMed: 9403622]
2. Grossman W, Jones D, McLaurin LP. Wall stress and patterns of hypertrophy in the human left ventricle. J Clin Invest 1975;56(1):56–64. [PubMed: 124746]
3. Hammermeister KE, DeRouen TA, Dodge HT. Variables predictive of survival in patients with coronary disease. Selection by univariate and multivariate analyses from the clinical, electrocardiographic, exercise, arteriographic, and quantitative angiographic evaluations. Circulation 1979;59(3):421–30. [PubMed: 761323]

4. Lee TH, Hamilton MA, Stevenson LW, et al. Impact of left ventricular cavity size on survival in advanced heart failure. Am J Cardiol 1993;72(9):672–6. [PubMed: 8249843]
5. Wong M, Johnson G, Shabetai R, et al. Echocardiographic variables as prognostic indicators and therapeutic monitors in chronic congestive heart failure. Veterans Affairs cooperative studies V-HeFT I and II. V-HeFT VA Cooperative Studies Group. Circulation 1993;87(6 Suppl):VI65–70. [PubMed: 8500242]
6. Kass DA, Baughman KL, Pak PH, et al. Reverse remodeling from cardiomyoplasty in human heart failure. External constraint versus active assist. Circulation 1995;91(9):2314–8. [PubMed: 7729016]
7. Acker MA, Bolling S, Shemin R, et al. Mitral valve surgery in heart failure: insights from the Acorn Clinical Trial. J Thorac Cardiovasc Surg 2006;132(3):568–77. 577, e1–4. [PubMed: 16935112]
8. Magovern JA. Experimental and clinical studies with the Paracor cardiac restraint device. Semin Thorac Cardiovasc Surg 2005;17(4):364–8. [PubMed: 16428045]
9. Ghanta RK, Rangaraj A, Umakanthan R, et al. Adjustable, physiological ventricular restraint improves left ventricular mechanics and reduces dilatation in an ovine model of chronic heart failure. Circulation 2007;115(10):1201–10. [PubMed: 17339543]
10. Blom AS, Mukherjee R, Pilla JJ, et al. Cardiac support device modifies left ventricular geometry and myocardial structure after myocardial infarction. Circulation 2005;112(9):1274–83. [PubMed: 16129812]
11. Cheng A, Nguyen TC, Malinowski M, et al. Passive ventricular constraint prevents transmural shear strain progression in left ventricle remodeling. Circulation 2006;114(1 Suppl):I79–86. [PubMed: 16820650]
12. Pilla JJ, Blom AS, Brockman DJ, et al. Ventricular constraint using the acorn cardiac support device reduces myocardial akinetic area in an ovine model of acute infarction. Circulation 2002;106(12 Suppl 1):I207–11. [PubMed: 12354735]
13. Ghanta RK, Lee LS, Umakanthan R, et al. Real-time adjustment of ventricular restraint therapy in heart failure. Eur J Cardiothorac Surg 2008;34(6):1136–40. [PubMed: 18715793]
14. Sabbah HN, Shimoyama H, Kono T, et al. Effects of long-term monotherapy with enalapril, metoprolol, and digoxin on the progression of left ventricular dysfunction and dilation in dogs with reduced ejection fraction. Circulation 1994;89(6):2852–9. [PubMed: 8205701]
15. Sabbah HN, Stein PD, Kono T, et al. A canine model of chronic heart failure produced by multiple sequential coronary microembolizations. Am J Physiol 1991;260(4 Pt 2):H1379–84. [PubMed: 1826414]
16. Sabbah HN, Sharov VG, Gupta RC, et al. Reversal of chronic molecular and cellular abnormalities due to heart failure by passive mechanical ventricular containment. Circ Res 2003;93(11):1095–101. [PubMed: 14563716]
17. Streeter DD Jr, Hanna WT. Engineering mechanics for successive states in canine left ventricular myocardium. II. Fiber angle and sarcomere length. Circ Res 1973;33(6):656–64. [PubMed: 4762007]
18. Guccione JM, Costa KD, McCulloch AD. Finite element stress analysis of left ventricular mechanics in the beating dog heart. J Biomech 1995;28(10):1167–77. [PubMed: 8550635]
19. Guccione JM, Waldman LK, McCulloch AD. Mechanics of active contraction in cardiac muscle: Part II--Cylindrical models of the systolic left ventricle. J Biomech Eng 1993;115(1):82–90. [PubMed: 8445902]
20. Lin DH, Yin FC. A multiaxial constitutive law for mammalian left ventricular myocardium in steady-state barium contracture or tetanus. J Biomech Eng 1998;120(4):504–17. [PubMed: 10412422]
21. Usyk TP, Mazhari R, McCulloch AD. Effect of laminar orthotropic myofiber architecture on regional stress and strain in the canine left ventricle. J Elasticity 2000;61:143–64.
22. Walker JC, Ratcliffe MB, Zhang P, et al. MRI-based finite-element analysis of left ventricular aneurysm. Am J Physiol Heart Circ Physiol 2005;289(2):H692–700. [PubMed: 15778283]
23. Kleinbaum, D.; Kupper, L.; Muller, K. Applied regression analysis and other multivariable methods. Boston: PWS-Kent; 1988.
24. Suga H. Total mechanical energy of a ventricle model and cardiac oxygen consumption. Am J Physiol 1979;236(3):H498–505. [PubMed: 426086]

25. Murakami T, Kikugawa D, Endou K, et al. Changes in patterns of left ventricular hypertrophy after aortic valve replacement for aortic stenosis and regurgitation with St. Jude Medical cardiac valves. Artif Organs 2000;24(12):953–8. [PubMed: 11121975]

26. Soman P, Pandian NG, Fiore J, Homoud M, Konstam MA. Reversal of left ventricular remodeling by pericardial tamponade. J Card Fail 2005;11(2):131–3. [PubMed: 15732033]

27. Walsh RG. Design and features of the Acorn CorCap Cardiac Support Device: the concept of passive mechanical diastolic support. Heart Fail Rev 2005;10(2):101–7. [PubMed: 16258717]

28. Humphrey, JD. Cardiovascular solid mechanics : cells, tissues, and organs. New York: Springer; 2002. p. xvip. 757

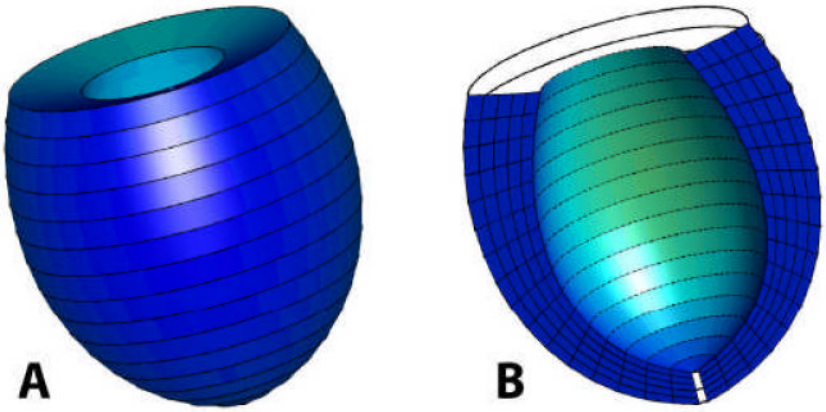

Figure 1.
(A) 3-dimensional finite element mesh of the unloaded dilated canine LV, 16x5x1 (longitudinal x transmural x circumferential), (B) cut away view of the interior cavity and wall cross-section.

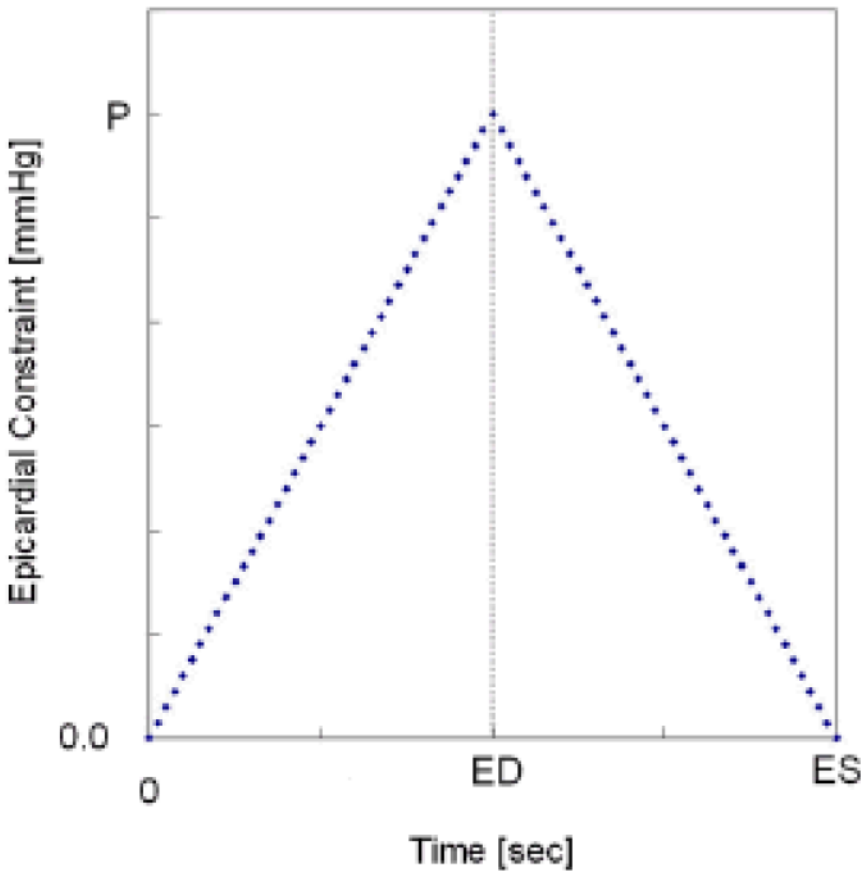

Figure 2.
Epicardial pressure loading profile; P = 3, 5, 7, and 9 mmHg (Time points for ED and ES are not drawn to scale).

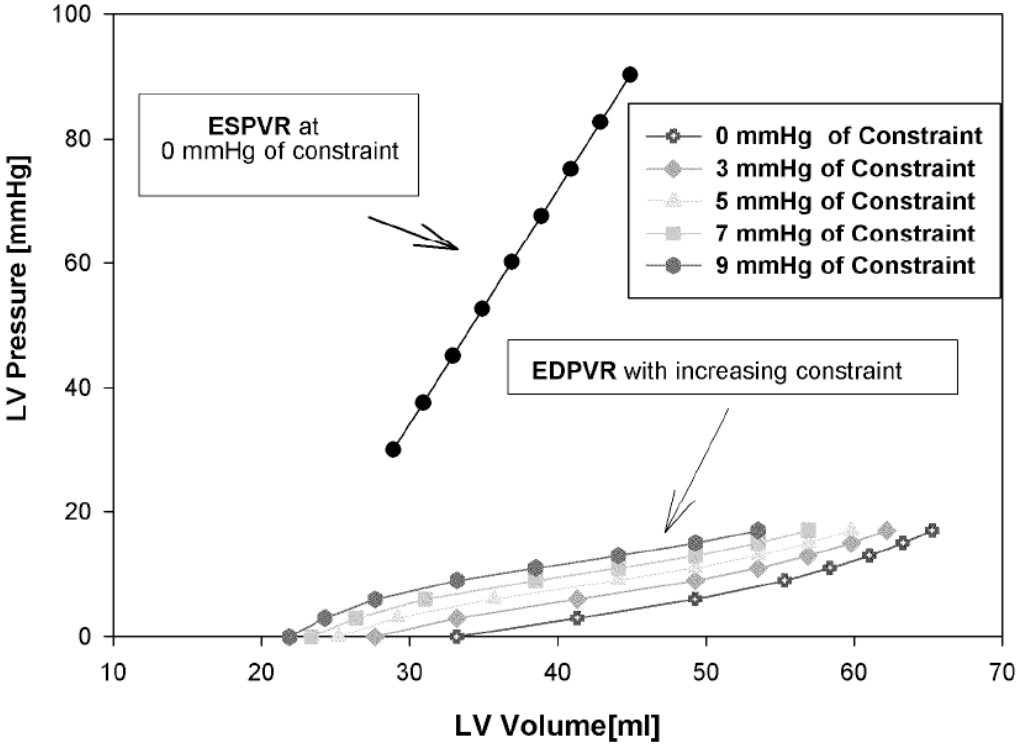

Figure 3.
The effect of constraint on end-diastolic compliance; at baseline, 3, 5, 7, and 9 mmHg of constraint. The compliance is shifted to the left as the level of passive constraint increases.

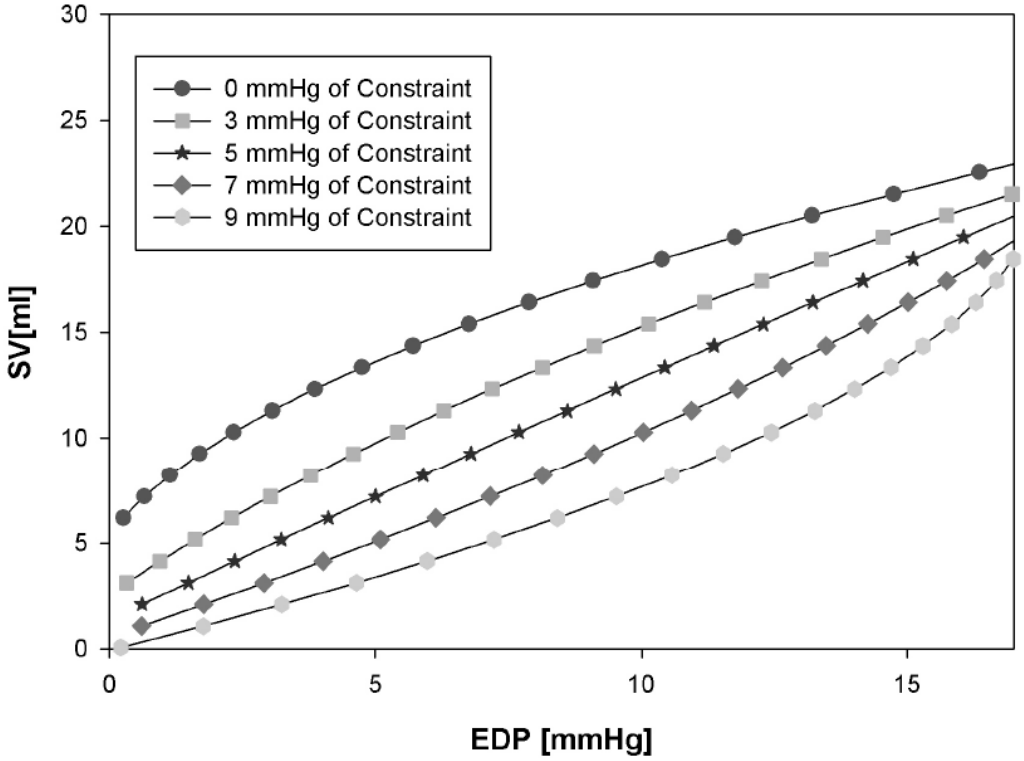

Figure 4.
The effect of adjustable passive constraint on the stroke volume/end-diastolic pressure (Starlings) relationship at baseline, 3, 5, 7, and 9 mmHg of constraint.

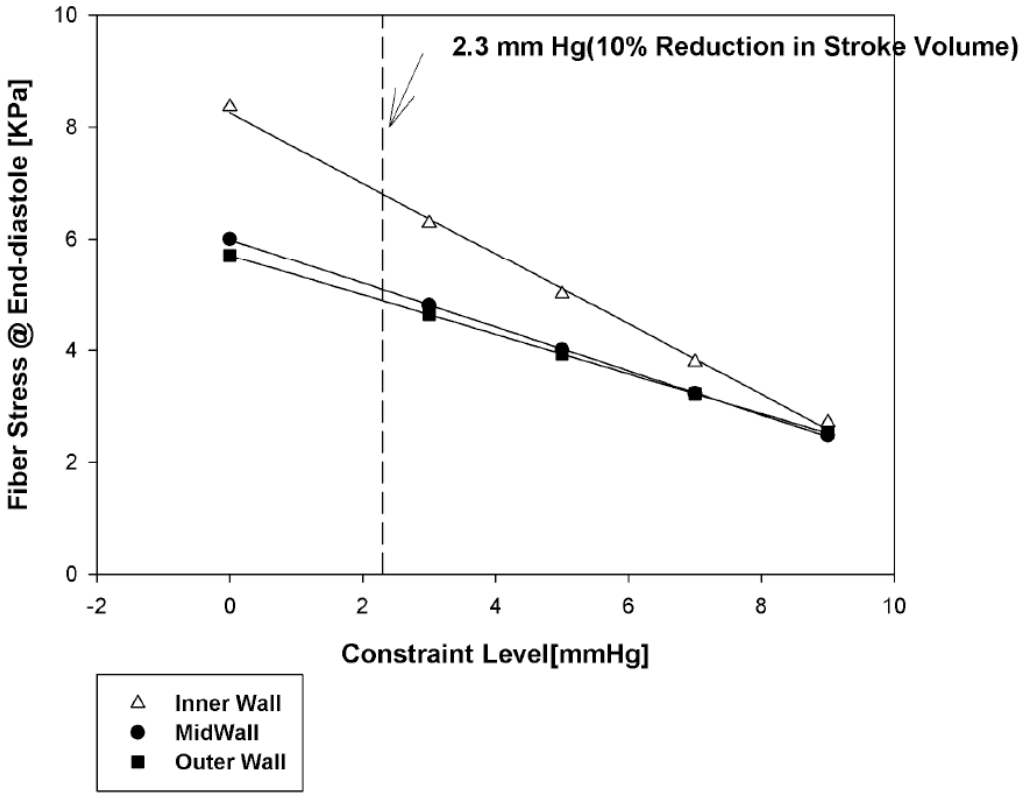

Figure 5.

Mean volume weighted end-diastolic fiber stress; as the level of passive constraint increases. Fiber stress at end-diastole was reduced by 18.3% (Inner wall), 15.3% (Mid wall), and 14.2% (Outer wall) at a constraint level of 2.3 mmHg.

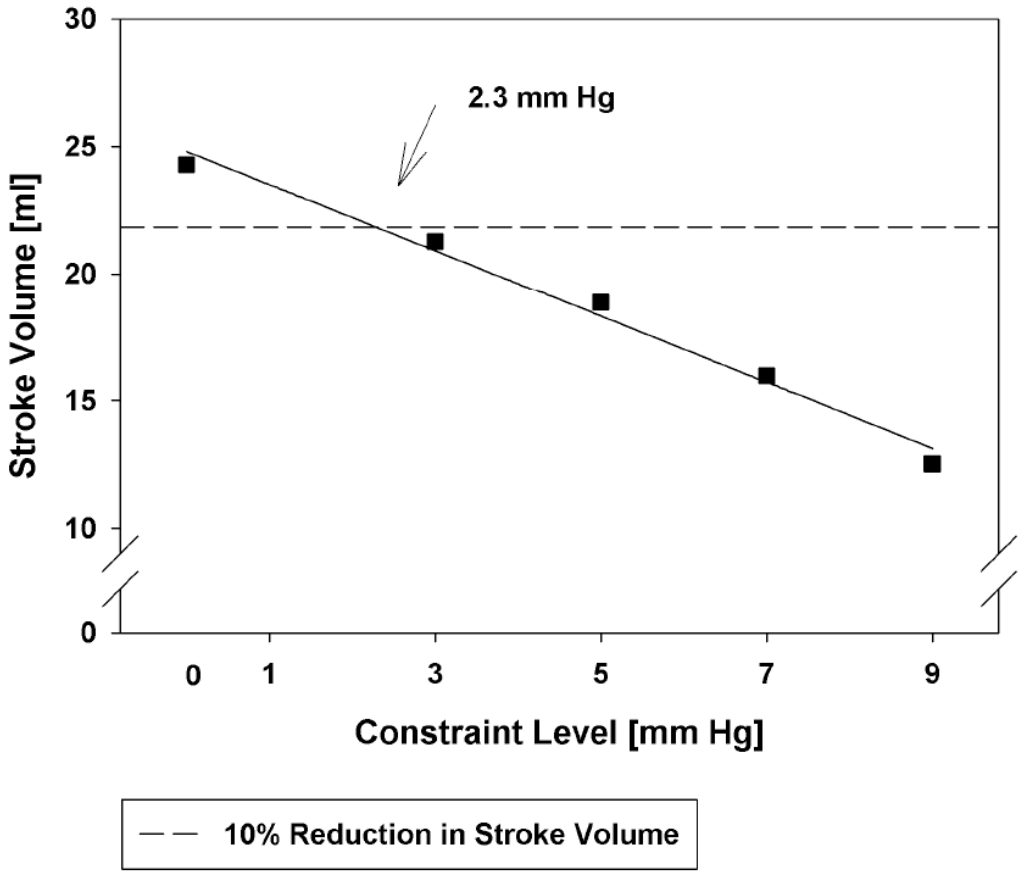

Figure 6.
Relationship between stroke volume at initial end-diastolic pressure (17 mm Hg). Note that any amount of constraint is associated with a reduction in stroke volume. A line of 10% reduction in stroke volume occurs at 2.3 mmHg.

Table 1

The effect of adjustable passive constraint on end-diastolic volume (EDV) and ejection fraction (EF).

Level of Constraint	EDV [ml]	EF [%]
0 mmHg	65.27	31.20
3 mmHg	62.22	27.83
5 mmHg	59.80	24.91
7 mmHg	56.91	21.09
9 mmHg	53.51	16.07

Table 2

The effect of adjustable passive constraint on diastolic compliance.

Level of Constraint	Diastolic compliance		
	β0	β1	β2
0 mmHg	5.4263	-0.4913	0.0101
3 mmHg	-4.5500	0.0601	0.0045
5 mmHg	-9.8051	0.4009	0.0006
7 mmHg	-14.8980	0.7584	-0.0037
9 mmHg	-20.4283	1.1735	-0.0091